Numerical study of tearing mode seeding in tokamak X-point plasma

Dmytro Meshcheriakov, Matthias Hoelzl (iD), Valentin Igochine (iD), Sina Fietz, Francois Orain (iD), Guido T. A. Huijsmans (iD), Marc Maraschek, Mike Dunne, Rachael McDermott (iD), Hartmut Zohm (iD), Karl Lackner, Sibylle Günter, ASDEX Upgrade Team, and EUROfusion MST1 Team

View Online   Export Citation   CrossMark

ARTICLES YOU MAY BE INTERESTED IN

Where in the world is AIP Publishing?
Find out where we are exhibiting next

AIP Publishing

Numerical study of tearing mode seeding in tokamak X-point plasma

View Online   Export Citation   CrossMark

Dmytro Meshcheriakov,[1,2,a)] Matthias Hoelzl,[1] Valentin Igochine,[1] Sina Fietz,[1] Francois Orain,[1,3]
Guido T. A. Huijsmans,[4,5] Marc Maraschek,[1] Mike Dunne,[1] Rachael McDermott,[1] Hartmut Zohm,[1]
Karl Lackner,[1] Sibylle Günter,[1] ASDEX Upgrade Team[1] and EUROfusion MST1 Team[b)]

AFFILIATIONS

[1]Max Planck Institute for Plasma Physics, Boltzmannstr. 2, 85748 Garching b.M., Germany
[2]Max-Planck/Princeton Research Center for Plasma Physics
[3]CPHT, Ecole Polytechnique, 91128 Palaiseau Cedex, France
[4]CEA Cadarache, IRFM, 13108 St. Paul Lez Durance Cedex, France
[5]Technische Universiteit Eindhoven, P.O. Box 513, 5600 MB Eindhoven, The Netherlands

[a)]dmytro.meshcheriakov@ipp.mpg.de
[b)]See author list of MST1 Team in H. Meyer *et al.*, Nucl. Fusion **57**, 102014 (2017).

ABSTRACT

A detailed understanding of island seeding is crucial to avoid neoclassical tearing modes and their negative consequences like confinement degradation and disruptions. In the present work, we investigate the growth of 2/1 islands in response to magnetic perturbations. Although we use externally applied perturbations produced by resonant magnetic perturbation (RMP) coils for this study, the results are directly transferable to island seeding by other MHD instabilities creating a resonant magnetic field component at the rational surface. Experimental results for 2/1 island penetration from ASDEX Upgrade are presented extending previous studies. Simulations are based on an ASDEX Upgrade L-mode discharge with low collisionality and active RMP coils. Our numerical studies are performed with the 3D, two-fluid, nonlinear MHD code JOREK. All three phases of mode seeding observed in the experiment are also seen in the simulations: first, a weak response phase characterized by large perpendicular electron flow velocities followed by a fast growth of the magnetic island size accompanied by a reduction of the perpendicular electron velocity and finally the saturation to a fully formed island state with perpendicular electron velocity close to zero. Thresholds for mode penetration are observed in the plasma rotation as well as in the RMP coil current. A hysteresis of the island size and electron perpendicular velocity is observed between the ramping up and down of the RMP amplitude consistent with an analytically predicted bifurcation. The transition from dominant kink/bending to tearing parity during the penetration is investigated.

Published under license by AIP Publishing. https://doi.org/10.1063/1.5086402

I. INTRODUCTION

Physics of forced magnetic reconnection in magnetically confined plasmas is crucial to understand magnetic island formation and associated degradation of the plasma confinement and potentially a disruption of the plasma. An instability associated with magnetic reconnection develops in the presence of finite plasma resistivity or other nonideal effects and is driven by both the equilibrium current density gradient (classical tearing mode) and a "hole" in the bootstrap current profile (neoclassical tearing mode or NTM)[1–4] caused by a flattening of the temperature distribution inside the magnetic island.[5]

It was shown both theoretically[3,6–10] and experimentally[4,11–15] that NTMs are linearly stable and require a seed magnetic island for their growth which is provided by triggers like other MHD instabilities. Resistive MHD predicts tearing modes to be linearly unstable when the parameter Δ', measuring the available magnetic free energy, is positive. Two-fluid pressure gradient effects, the ion polarization current and the toroidal curvature, the so-called Glasser-Greene-Johnson effect, provide additional stabilizing effects.[16–18] When a tearing mode is linearly stable, a sufficiently large initial seed island can lead to further island growth since it causes a helical perturbation of the temperature distribution and consequently the bootstrap current, which acts destabilizing. Nonlinear effects and toroidal mode coupling enable the generation of a seed island from an initial perturbation with a different helicity. For example, sawtooth postcursors with

helicity $m/n = 1/1$ were observed[11,14] to produce a 2/1 component acting as a seed for a 2/1 magnetic island.

A basic theoretical framework of tearing mode interactions with a static external magnetic perturbation in cylindrical geometry is proposed by Fitzpatrick.[19] In this work, externally applied MPs are treated as modified edge boundary conditions. The interaction of the external MPs with the helical perturbation current associated with a magnetic island results in the modification of the island width evolution and a rise of a local $\mathbf{j} \times \mathbf{B}$ torque in the vicinity of the island. If the island frequency deviates from its natural frequency, the plasma exerts a viscous restoring torque onto the island. The general nonlinear tearing mode stability problem is then treated as a balance of the plasma inertia in the island and the sum of the local electromagnetic and viscous torques. In the presence of perpendicular electron velocity, static resonant magnetic perturbations (RMPs) in the laboratory frame correspond to time varying RMPs in the electron fluid frame and therefore induce a current hindering their penetration.[20,21]

A steady state is obtained when the viscous torque is balanced by the electromagnetic one. Solutions corresponding to different values of initial plasma rotation (and, as a result, island natural frequency) are shown in Fig. 1. For large initial plasma rotation, a bifurcation is observed and the plasma undergoes a sudden transition at about half the initial rotation frequency to a nonlinear island state, characterized by low plasma rotation and a large magnetic island. This transition is generally called mode penetration. Due to the bifurcation, a hysteresis is expected for the back transition: The island remains on the lower branch of the figure in the region where the force balance equation does not have a unique solution.
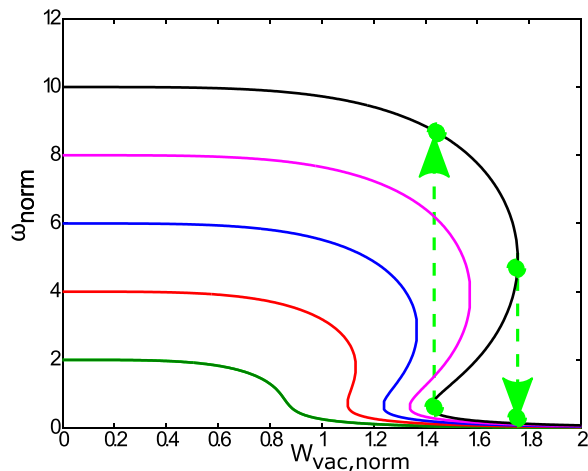

FIG. 1. The steady state mode rotation frequency is plotted vs the applied perturbation amplitude according to analytical theory (see Ref. 19, also for the normalization). The different curves correspond to different background rotation values, i.e., different rotation frequencies in the absence of the perturbation. At high rotation frequencies, a bifurcation is observed, where the force balance does not have a unique solution any more. Finally, when the rotation frequency has dropped by a factor of about two, the plasma can undergo a fast transition to the penetrated state with a rotation frequency close to zero. A hysteresis of rotation frequency (and correspondingly penetrated island size) is expected between a ramping up and down of the perturbation amplitude except for low background rotation where the solution remains unique for all perturbation amplitudes.

In the present paper, the seeding of a tearing mode by externally applied magnetic perturbations is studied in the presence of realistic poloidal and toroidal background rotation. The successive mode evolution and the impact on confinement are also addressed. These questions are investigated with the toroidal nonlinear MHD code JOREK,[22,23] which includes anisotropic heat transport, two-fluid diamagnetic effects,[24] neoclassical friction, and toroidal rotation in realistic tokamak X-point geometry. A discharge in low density L-mode plasmas[25] in the ASDEX Upgrade[26] tokamak (AUG#30734) was chosen as basis for our studies. Bootstrap current drive is not considered in the present work since we are predominantly interested in the seeding, respectively, mode penetration, not the further nonlinear evolution. Also, the effect of neoclassical toroidal viscosity (NTV), which would enhance mode penetration, is not taken into account in the present paper. Inclusion of NTV and bootstrap current as well as quantitative comparisons to the experiment is left for future studies.

This paper is organized as follows: In Sec. II, we briefly show experimental observations from ASDEX Upgrade. Section III introduces the JOREK code, the simulation setup, and results of our simulations of 2/1 mode penetration in ASDEX Upgrade reproducing qualitatively all experimental observations and analytical predictions. This includes observations of penetration thresholds in coil current and background rotation velocity, a hysteresis between ramp-up and ramp-down, and a transition from kink to tearing parity at the resonant surface. Summary and conclusions are given in Sec. IV.

II. MODE PENETRATION IN ASDEX UPGRADE EXPERIMENTS

Experimental results are shown in this section extending previous work described in Ref. 27. Here, we refer to the ASDEX Upgrade discharge number #30734. Three distinguished phases were observed in this experiment, while the current in the MP field coils with the dominant mode number $n = 1$ was slowly ramped up (Fig. 2).

In the first phase, denoted as the weak plasma response phase, the plasma response follows the amplitude of the magnetic perturbation approximately linearly. In this phase, screening is strong and the residual perturbation on the resonant surface is not sufficient to drive
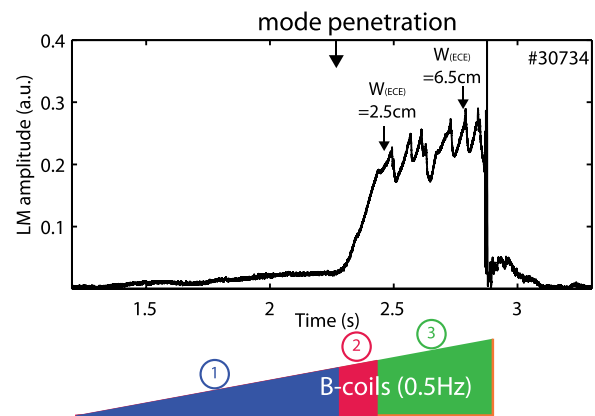

FIG. 2. Amplitude of the $n = 1$ magnetic field perturbation measured by the locked mode detection system and evolution of the current in the B-coils (below). The weak response phase (1), the penetration phase (2), and the saturation phase (3) are clearly visible.

magnetic reconnection. In the second phase, the perturbation exceeds a certain threshold and becomes strong enough to slow down the rotation strong enough such that the transition point is reached and forced reconnection takes place at the $q = 2$ surface. The resulting (2/1) magnetic island is observed in the magnetic data and in the electron temperature. In the third phase, the island growth slows down and is interrupted by some minor disruptions.

During the first phase (Fig. 3), the core toroidal rotation[29] decreases up to the point of mode penetration. A fast drop is observed in the second phase and the value remains almost constant during the whole third phase. The perpendicular electron velocity is calculated from the measured $E \times B$ velocity and the electron diamagnetic drift velocity. The $E \times B$ velocity is evaluated from the Er profile measured with charge exchange recombination spectroscopy via the radial force
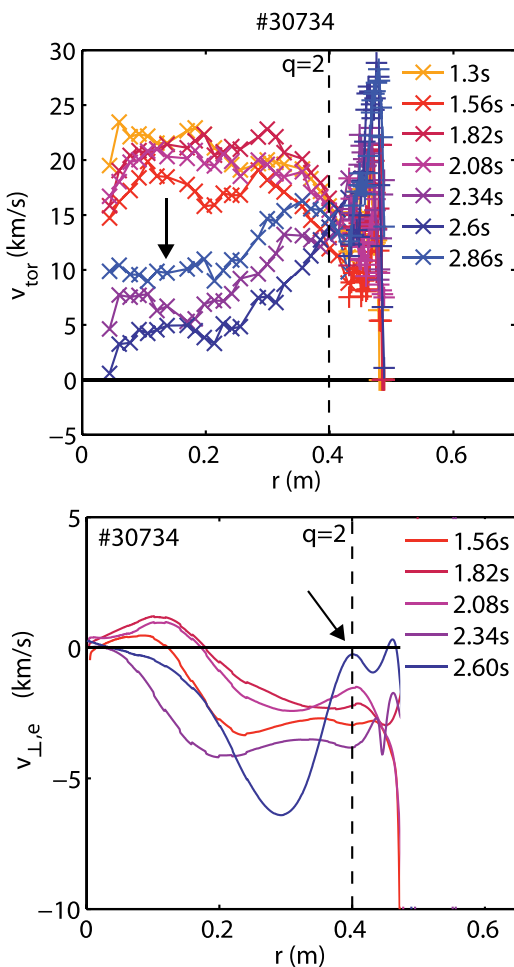

FIG. 3. Experimental toroidal rotation (upper) and perpendicular electron velocity (lower) profiles measured by charge exchange recombination spectroscopy[28] at several time points of the experiment shown in Fig. 2. The toroidal rotation velocity is reduced after the penetration in the plasma core. The perpendicular electron velocity drops to zero at the $q = 2$ surface when the 2/1 mode is fully penetrated. Fast penetration approximately sets in when the original perpendicular electron velocity has dropped by a factor of two consistent with the analytical predictions described above.

balance equation, while the electron diamagnetic drift velocity is calculated from the measured electron temperature and density profile. In the plasma core, the toroidal rotation velocity is the dominant term in the radial force balance equation and hence, we have used this term in the radial force balance equation to evaluate the $E \times B$ velocity. Further information about the measurements in ASDEX Upgrade is found for instance in Ref. 30. In the first phase, the motion of the electron fluid across the field lines at the resonant surfaces screens the RMPs hindering their penetration in agreement with previous findings that the electron perpendicular rotation is a key factor for the screening of magnetic perturbations by the plasma.[24,31–33] Mode penetration corresponds to a drop of the perpendicular electron velocity to approximately zero. These experiments confirm the predicted slow decrease in the plasma rotation towards the time of mode penetration and the small electron perpendicular velocity when an island is formed. The onset of mode penetration approximately takes place when the perpendicular electron velocity at the rational surface has dropped by a factor of two consistent with analytical predictions.

A set of experiments to study the impact of the perturbation amplitude onto mode seeding was performed. The results of these experiments are shown in Fig. 4. The signals of the locked mode detector on the upper part of the plot are shifted in order to match the time of mode penetration across all experiments. The shapes of current amplitude in the RMP coils in the lower part of the Figure are shifted accordingly. The time delay of mode penetration with respect to the RMP ramp-up time increases for lower coil currents, i.e., for lower perturbation amplitudes. Ultimately, when the RMP current becomes too small, no penetration is observed at all. Thus, a threshold in the coil currents is observed for mode penetration (between 100 and 200 A in this case), below which the $j \times B$ torque does not reduce the perpendicular electron velocity strong enough to reach the transition point.

III. NON-LINEAR SIMULATIONS OF MODE PENETRATION IN ASDEX UPGRADE

In the following, we present simulation results for mode penetration by externally applied resonant magnetic perturbations. This section is organized as follows. In Sec. III A, the nonlinear MHD code JOREK used for the simulations is briefly described and the simulation setup is explained in Sec. III B. An overview of all simulations performed is given in Sec. III C.

Section III D shows results for a simulation of an ASDEX Upgrade like plasma. All three phases of mode penetration can be seen in this simulation consistent with experiments and analytical theory. Also the evolution of toroidal and poloidal rotation is reproduced qualitatively. Section III E shows results of parameter scans in mode rotation and the coil currents revealing thresholds for mode penetration in both parameters. A hysteresis in island size and plasma rotation between ramp-up and ramp-down of the magnetic perturbation is observed in Sec. III F consistent with analytical predictions. Finally, Sec. III G investigates the evolution of the kink and tearing responses during mode penetration.

A. Physics model and JOREK nonlinear MHD code

Our simulations are performed with the 3D nonlinear MHD code JOREK[22] which is routinely applied to a variety of edge localized mode (ELM) and disruption related questions in tokamak X-point
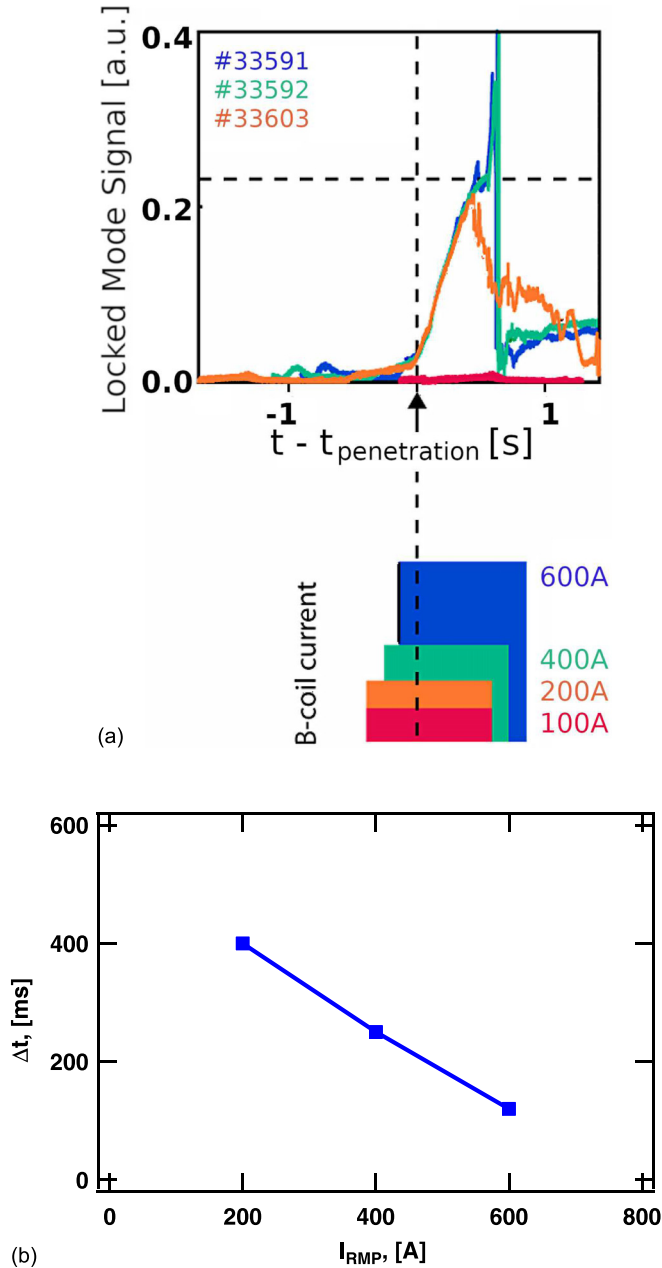
(a)

(b)

FIG. 4. Dependence of the mode penetration delay on the RMP current amplitude. For larger perturbation amplitudes, the mode penetration takes place faster. Delays are approximately 120 ms for 600 A, 250 ms for 400 A and 400 ms for 200 A. At a coil current of 100 A, no mode penetration is observed at all.

plasmas and has already been used for penetration studies of external magnetic perturbations.[20,21,34] The code uses 2D bi-cubic Bézier finite elements in the poloidal plane and a Fourier expansion in the toroidal direction.[23] The physics model used for our investigations is a resistive reduced-MHD[35,36] model with extensions[24] for two-fluid effects, realistic neoclassical poloidal rotation, and realistic toroidal background

rotation. The main reduced-MHD assumption is that the magnetic field is expressed as $\mathbf{B} = F_0/R\,\mathbf{e}_\phi + R^{-1}\,\nabla\Psi \times \mathbf{e}_\phi$, where $F_0 = R_0 B_{\phi 0}$ is constant in time and space, R_0 is the major radius, Ψ is the poloidal flux, $B_{\phi 0}$ is the toroidal magnetic field amplitude at the magnetic axis, and ϕ is the toroidal coordinate. The basic set of equations solved implicitly in the code includes the continuity equation, the parallel and perpendicular components of the momentum equation, the energy conservation equation, Ohm's law, and definition equations for the current and the vorticity. Two-fluid diamagnetic effects are included in the system via the diamagnetic velocity $\mathbf{V}_s^* = -\nabla P_s \times \mathbf{B}/(\rho e_s B^2/m_i)$ of each species s - electrons and ions. Here, P_s is the pressure of the species s and $\rho = m_i n$ is the mass density of the plasma; since electrons are much lighter than ions, the electron contribution is neglected; $n = n_i = n_e$ is the particle density, assuming the quasineutrality condition and singly charged ions. $e_s = \pm e$ denotes the electric charge of each species, and m_i is the ion mass. The fluid velocity is the sum of the $\mathbf{E} \times \mathbf{B}$ drift velocity $\mathbf{V}_E = \mathbf{E} \times \mathbf{B}/B^2$ and the parallel and ion diamagnetic velocities

$$\mathbf{V} \approx \mathbf{V}_i = \mathbf{V}_{\|,i} + \mathbf{V}_E + \mathbf{V}_i^*. \tag{1}$$

Neoclassical effects are considered in the momentum equation, where the pressure tensor is given by $\bar{P} = \bar{I}P + \bar{\Pi}_{i,neo} + \bar{\Pi}_{i,gv}$. After gyroviscous cancelation[37] and adopting the expression for the divergence of the neoclassical tensor derived by Gianakon et al[38]

$$\nabla \cdot \bar{\Pi}_{i,neo} = \rho\mu_{i,neo}\frac{B^2}{B_\theta^2}(V_\theta - V_{\theta,neo})\mathbf{e}_\theta, \tag{2}$$

with $\mu_{i,neo}$ being the neoclassical friction and $V_{\theta,neo} = -\kappa_i \nabla T_i \times \mathbf{B}/eB^2 \cdot \mathbf{e}_\theta$, where κ_i is the neoclassical heat diffusivity, the final set of model equations reads

$$\frac{\partial \rho}{\partial t} = -\nabla \cdot (\rho\mathbf{V}) + \nabla \cdot (D_\perp \nabla_\perp \rho) + S_\rho, \tag{3}$$

$$\rho\frac{\partial V_{\|,i}}{\partial t} = \mathbf{b} \cdot \left[-\rho((\mathbf{V}_{\|,i} + \mathbf{V}_E) \cdot \nabla)\mathbf{V} - \nabla P - \nabla \cdot \bar{\Pi}_{i,neo} \right]$$
$$+ \mu_\|\Delta(V_{\|,i} - V_{\|,\mathrm{NBI}}), \tag{4}$$

$$\mathbf{e}_\phi \cdot \nabla \times \left[\rho\frac{\partial \mathbf{V}_E}{\partial t} = -\rho(\mathbf{V} \cdot \nabla)\mathbf{V}_E + \mathbf{J} \times \mathbf{B} \right.$$
$$\left. -\nabla P - \nabla \cdot \bar{\Pi}_{i,neo} + \mu_\perp \Delta V \right], \tag{5}$$

$$\frac{\partial(\rho T)}{\partial t} = -\rho\mathbf{V_E} \cdot \nabla T - (\gamma - 1)P\nabla \cdot \mathbf{V_E}$$
$$+ \nabla \cdot (\kappa_\|\nabla_\| T + \kappa_\perp \nabla_\perp T) + S_T, \tag{6}$$

$$\frac{1}{R^2}\frac{\partial \psi}{\partial t} = -\mathbf{B} \cdot \nabla_\| u + \frac{\tau_{IC}}{\rho}\mathbf{B} \cdot \nabla_\| P + \frac{\eta}{R^2}(J - J_0), \tag{7}$$

with the parallel gradient defined as follows:

$$\nabla_\|\alpha = \mathbf{b}(\mathbf{b} \cdot \nabla\alpha) = \frac{\mathbf{b}}{B}\left(\frac{F_0}{R^2}\partial_\phi\alpha + \nabla\phi \cdot \nabla\alpha \times \nabla\psi\right). \tag{8}$$

In this system of equations, T denotes the temperature (assuming same temperature for ions and electrons), J is the toroidal current, u is the electrostatic potential, $D_\perp$ is the particle diffusion coefficient, $\mu_\|$ and $\mu_\perp$ are the parallel and perpendicular viscosity coefficients, γ

$= 5/3$ is the adiabatic index, $\kappa_\perp$ and $\kappa_\parallel$ are the perpendicular and parallel heat diffusivities, η is the resistivity, $\mathbf{b} = \mathbf{B}/B$ and $B = |\mathbf{B}|$ is the unit vector along the magnetic field, and $\mathbf{e}_\theta = \mathbf{b} \times \mathbf{e}_\phi$ is the poloidal unit vector. In the simulations, both the plasma resistivity and the viscosity evolve in time according to Spitzer-like $(T/T_0)^{3/2}$ dependence and the parallel heat diffusivity evolves as $(T/T_0)^{5/2}$, where T_0 is the initial temperature in the plasma center.

S_ρ and S_T are sources of particles and heat, respectively. The terms $V_{\parallel,\mathrm{NBI}}$ and J_0 drive the parallel rotation and the current density in the absence of an island towards the initial profiles by compensating the decay due to parallel viscosity and resistivity, respectively. The radial profile of heat and particle sources is assumed to be Gaussian. Source and diffusion profiles are adjusted to keep the density and temperature profiles close to the initial profiles in the absence of an instability, such that the steady state values and gradients of density and temperature remain close to the initial values in the region of interest, i.e., in the vicinity of the $q=2$ resonant surface. Note that the employed gyroviscous cancelation breaks the strict conservation of energy. Linear benchmarks have shown that growth rates are correct with our present model. Plans exist to implement a fully conservative model without this cancelation; however, this is left for future work. The Ohmic heating term is not accounted for in our simulations, since we take an artificially increased resistivity (see Sec. III B), which would lead to an unrealistic source of thermal energy. Instead the thermal energy is modeled via a Gaussian source.

The perturbation induced by RMP coils is modeled as the Dirichlet boundary condition for the poloidal magnetic flux. A pure $n=1$ perturbation is applied. The vacuum RMP spectrum is calculated at the boundary of the JOREK computational domain with an external program and applied as a Dirichlet boundary condition. RMPs are progressively switched on in time: the amplitude of the perturbation is gradually increased within a typical timescale $t \sim 1000\tau_A$, where $\tau_A = \sqrt{\mu_0\rho_0}$ approximates the Alfven time scale, μ_0 is the vacuum permeability, and ρ_0 is the mass density in the plasma center. For the plasma parameters of our equilibrium, $\tau_A = 0.6\ \mu$s. In this way, the magnetic perturbation gradually penetrates into the plasma, which self-consistently adapts in the process. The choice of the RMP timescale was taken for numerical reasons and is not consistent with the experimental ordering with typical visco-resistive and toroidal rotation times; however, this does not affect our physical results as we have checked by varying the ramp-up function.

B. Simulation setup

In our simulations, JOREK is initialized for an ASDEX Upgrade like plasma: major radius $R \approx 1.65$ m, minor radius $a \approx 0.5$ m, toroidal field strength on axis $B_t = 1.9$ T, plasma current $I_p = 1$ MA, and edge safety factor $q_{95} = 3.8$. The full X-point plasma including the scrape-off layer up to simplified divertor targets is included in the simulation domain. The central electron density is $n_{e,0} = 8 \times 10^{19}$ m^{-3}; the central temperature is $T_{e,0} = 1$ keV. The perpendicular heat diffusion coefficient is in the range $\chi_\perp \sim 0.5$ m^2/s. The parallel heat diffusion coefficient is proportional to $T_e^{5/2}$ with the value $\chi_\parallel \sim 3.5 \times 10^8$ m^2/s at the plasma center chosen to be about one order of magnitude lower than Spitzer-Härm predictions[39] since typically the heat flux limit[40] reduces the parallel conductivity in the experiment.[41] RMP currents are chosen around $I_{RMP} \sim 1$ kA and scanned in a few simulations. The perpendicular electron background velocity is modified by

changing the toroidal rotation velocity. Input profiles are given in Figs. 5 and 6. Input heat and particle diffusion profiles are shown in Fig. 7. The Lundquist number $S = \frac{\mu_0 a v_{\mathrm{Alfven}}}{\eta} \approx 1 \times 10^7$ in the simulations is close to experimental conditions. The magnetic Prandtl number is chosen to be constant across the whole simulation domain such that viscosity is close to the collisional value estimated from the experimental data $P_{rm} = \nu/\eta = (\mu/\rho_0)/\eta = 10$.

The most important effect missing in our simulations is the neo-classical toroidal viscosity, which would lead to a faster penetration of the magnetic perturbation and a penetration already at lower RMP coil currents or higher initial plasma rotation frequencies. We leave the implementation and study of this effect for future studies. A consistent evolution of the bootstrap current, which is available in the JOREK code for further studies, is also neglected since we are interested in particular in the seeding and penetration phases. In addition, the hysteresis effect investigated in Sec. III F can be studied this way independently of the bootstrap current term simplifying the interpretation of the results.

C. Overview of the simulations performed

In the following, we give a brief overview of the simulations performed for this paper and refer to the respective sections, in which the results are discussed in detail.
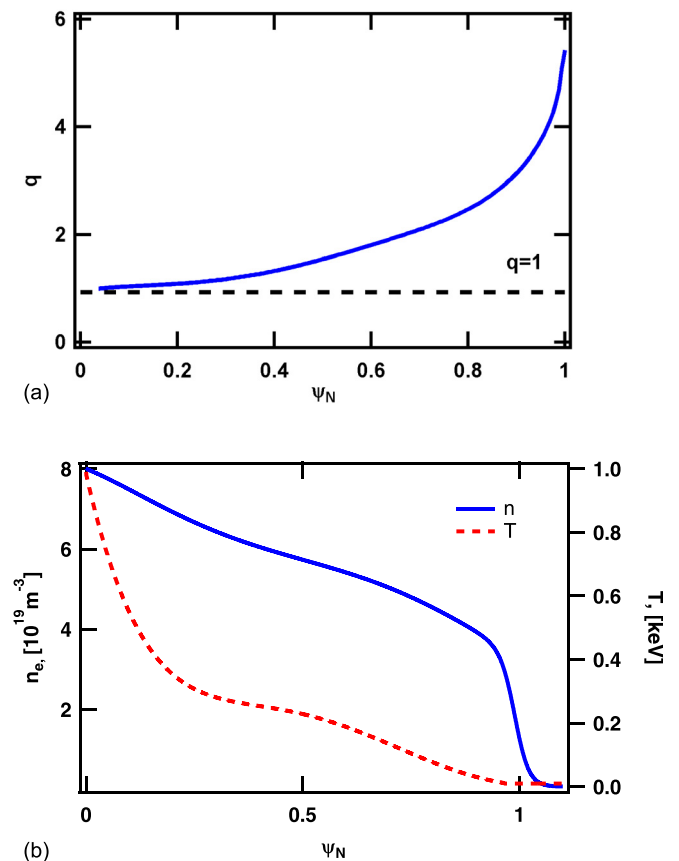

(a)

(b)

FIG. 5. Profiles of the safety factor q (top) and the density and temperature (bottom). All simulation input is based on the CLISTE equilibrium reconstruction for ASDEX Upgrade L-Mode discharge #30734 at 1.2 s.
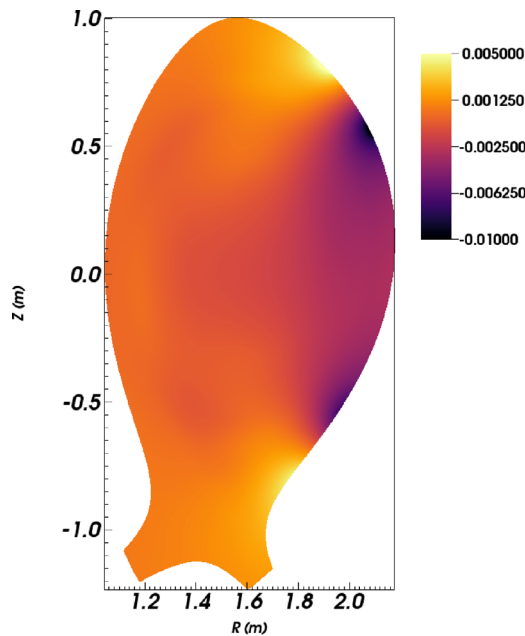
FIG. 6. The vacuum poloidal flux is prescribed at the boundary of the computational domain for simulating the RMP coils.

Simulations at fully realistic Lundquist number for ASDEX Upgrade L-Mode experiments have been performed and reflect the qualitative change of the toroidal and electron perpendicular rotation profiles, however, full penetration was not obtained (very likely due to the missing NTV effects). Thus, all simulations shown in the following are performed with values reduced by about a factor three to $S = 1 \times 10^7$.

The typical process of mode seeding is shown and analyzed in Sec. III D. The initial toroidal velocity used in the simulations is $V_{tor} = 2.8$ km/s and RMP current $I_{RMP} = 2$ kA. The thresholds for mode seeding in perturbation amplitude and rotation are studied in

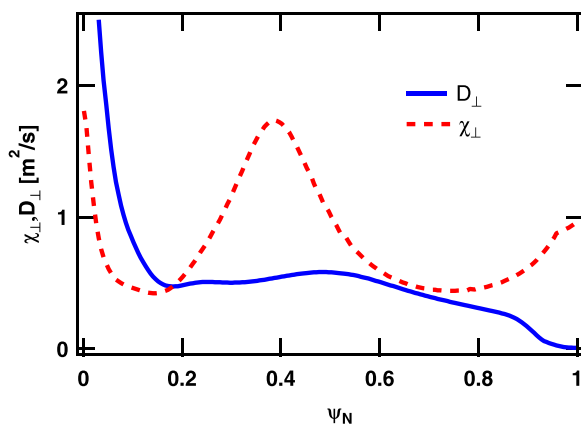**FIG. 7.** Profiles of the perpendicular heat and particle diffusivities used in the simulations. Note that $\chi_\perp$ is connected to $\kappa_\perp$ used in the model equations by $\chi_\perp = \kappa_\perp / \rho$ where ρ denotes the mass density.

TABLE I. Simulations performed for the scan in RMP current amplitude.

V_{tor}		I_{RMP}	
2.5 km/s	1.9 kA	2 kA	
6.2 km/s	2 kA	2.2 kA	2.4 kA

Sec. III E by means of the parameter scans shown in Tables I and II. The toroidal rotation was used as a proxy to modify the perpendicular electron velocity as shown in Table III.

Finally, simulations to study the hysteresis behavior between ramp-up and ramp-down of the RMP coil currents are shown in Sec. III F. These simulations were performed with $V_{tor} = 6.2$ km/s and the RMP current amplitudes shown in Table IV.

D. Typical simulation of mode penetration into an ASDEX Upgrade L-mode plasma

This section shows a typical simulation of mode penetration performed with $V_{tor} = 2.8$ km/s and $I_{RMP} = 2$ kA at $S = 10^7$. Like in the experimental observations shown in Sec. II, three phases are observed. First, the plasma exhibits a weak response to the applied perturbation. Once a specific threshold is reached (see Fig. 1), mode growth accelerates until the final mode saturation at low perpendicular electron velocity is obtained. Time traces for the evolution of the island size and the perpendicular electron velocity at the rational surface are shown in Figs. 8 and 9, respectively.

In the beginning, the island size is small and the perpendicular electron velocity at the rational surface is around $\sim$1.8 km/s. The electron velocity is given by $\mathbf{V}_e = \mathbf{E} \times \mathbf{B}/B^2 + \nabla p \times \mathbf{B}/(2 n_e e B^2) + \mathbf{V}_{\|,e}$, where the factor 2 is a result of the assumption of having the same electron and ion temperatures in the model employed here (a model treating both temperatures differently is available as well). The rotation velocity has dropped by a factor of two after approximately $t = 4100 \tau_A$ and an accelerated growth of the island (mode penetration) sets in at around $t = 4900 \tau_A$. The electron velocity comes to rest at the rational surface around $t = 6100 \tau_A$ and the saturation of the island starts around $t = 12\,000 \tau_A$. Figure 8 shows the time evolution for the square of the island width which is proportional to the current perturbation at the resonant surface and, consequently, approximately proportional to the expected signals in magnetic pick up coils. The figure also contains the prescribed evolution of the RMP coil currents. Note that it is coincidence that saturation of the prescribed coil currents and onset of mode penetration take place approximately at the same time for this particular case (as proven by other simulations in our scans). For the perpendicular electron velocity at the rational surface shown in Fig. 9, also radial profiles at several points in time are provided in Fig. 10. Profiles are shown in the beginning of the simulation, before mode penetration sets in, during mode penetration, and in the saturated island state.

TABLE II. Simulations performed for the scan in the plasma rotation.

I_{RMP}		V_{tor}, (km/s)	
2 kA	2.5	4.4	6.2

TABLE III. Correspondence of the values of perpendicular electron velocity $V_{\perp,e}$ at the $q = 2$ resonant surface to the values of toroidal background rotation V_{tor} used in the parameter scan.

V_{tor} (km/s)	2.5	4.4	6.2
$V_{\perp,e}$ (km/s)	2.7	3	3.3

TABLE IV. Simulations performed for the hysteresis studies.

	I_{RMP}				
Ramp-up	2 kA	2.2 kA	2.4 kA		
Ramp-down	2.2 kA	2 kA	1.9 kA	1.75 kA	1.5 kA	1 kA
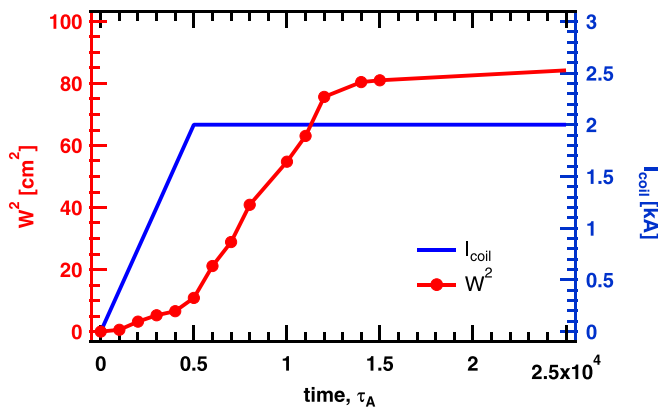
FIG. 8. Square of the island size (left axis) and current in the RMP coils (right axis).
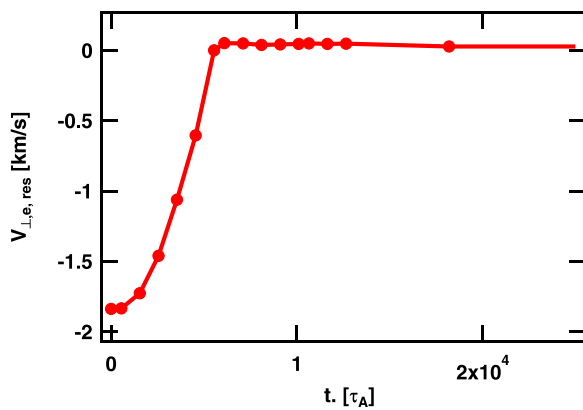

FIG. 9. Time evolution of the perpendicular electron velocity profiles from JOREK simulations with $S = 10^7$ at the $q = 2$ resonant surface.

Initially, the nonzero electron perpendicular velocity leads to the screening of the magnetic perturbation. However, the screening starts to drop due to the loss of the perpendicular component of the toroidal velocity (see Fig. 11) and flatting of the temperature (see Fig. 12)
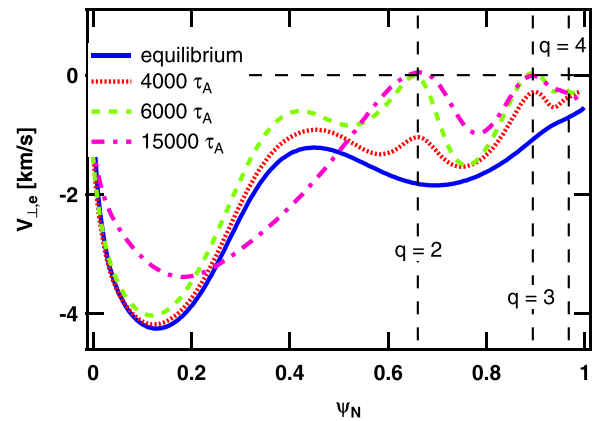

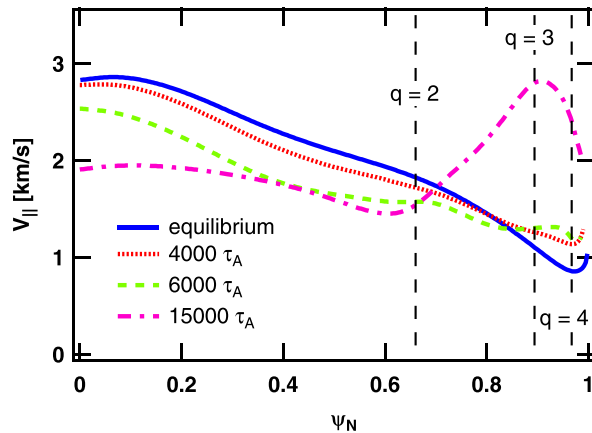**FIG. 10.** Perpendicular electron velocity profiles from JOREK simulations with $S = 10^7$.

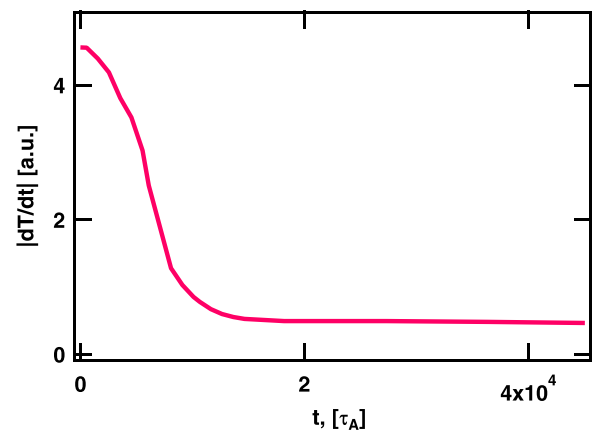**FIG. 11.** Toroidal rotation velocity profiles from JOREK simulations with $S = 10^7$.

FIG. 12. Time evolution of poloidally and toroidally averaged temperature gradient $dT/d\Psi_N$ at the $q = 2$ resonant surface.

leading to a partial loss of the diamagnetic component. Once the condition $V_{\perp,e} = 0$ is approximately satisfied, the transition phase is reached. In this phase, the perturbation propagates without screening forcing magnetic reconnection at the resonant surface. Similar to the experimental observations, the core toroidal velocity shown in Fig. 11 decreases.

Figure 13 finally shows Poincare plots of the magnetic topology before mode penetration sets in and in the saturated island state. A considerable stochastisation of the plasma edge, and a large 2/1 magnetic island can be seen.

E. Mode penetration thresholds in coil current and rotation velocity

Scans in both the plasma rotation velocity and the perturbation amplitude (coil currents) were carried out. The electron perpendicular velocity is modified in our scan by changing the toroidal velocity, while keeping the $\mathbf{E} \times \mathbf{B}$ and diamagnetic drift effects unchanged. Table III
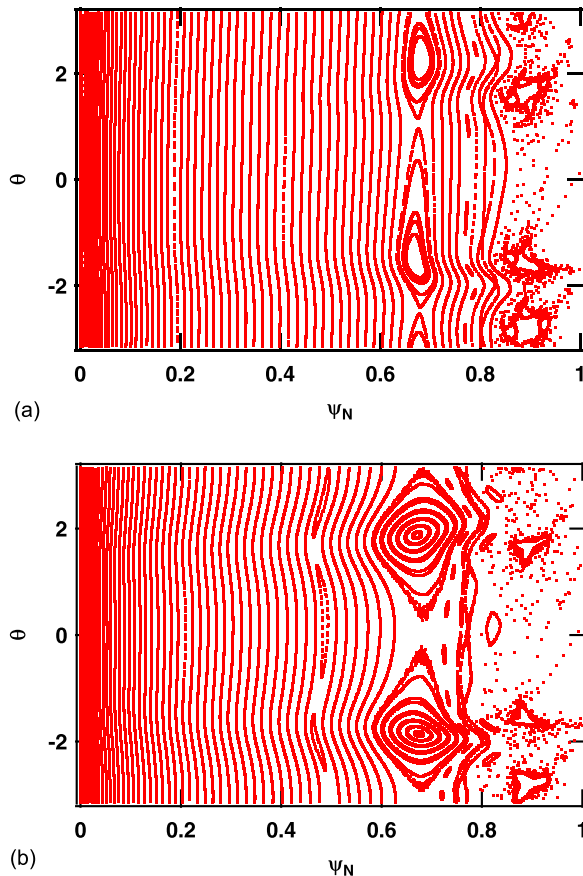

FIG. 14. Island size evolution for different values of the current in RMP coils at $V_{tor} = 2.5$ km/s.

shows how the perpendicular electron velocity is affected by our choice of the toroidal rotation velocity.

Scans in the perturbation amplitude for the values of toroidal velocity $V_{tor} = 2.5$ km/s and $V_{tor} = 6.2$ km/s are shown in Figs. 14 and 15, respectively. As the current in the RMP coils decreases, mode penetration slows down consistently with experimental observations (see Sec. II). Ultimately, if the perturbation is not strong enough, the electromagnetic torque cannot reduce the plasma rotation sufficiently to enter the penetration phase. The transition from a weak response phase to the fully formed island phase was observed experimentally.[25] Also, the time, required for the mode penetration, increased with the decrease in the RMP current. The threshold for the transition to the penetrated state can only be compared qualitatively to the experimental observations due to limitations of our model. In particular, we believe that the lack of Neoclassical Toroidal Viscosity (NTV) in the simulations is our biggest limitation as it would provide a localized decrease in the rotation of the mode.

The scan in the plasma rotation shows a delay in the mode penetration as the initial toroidal velocity increases as seen in Fig. 16. This

FIG. 13. Poincaré plots of the magnetic topology in (ψ_N, θ) coordinates before mode penetration $t = 4000\tau_A$ (upper plot) and in fully formed island phase $t = 15\,000\tau_A$ (lower plot). The width of the $q = 2$ island on the upper plot $W = 3.8$ cm and on the lower one $W = 9.2$ cm. The 3/1 and 4/1 islands penetrate faster than the 2/1 island since the applied spectrum contains significant 3/1 and 2/1 components and the electron velocity is slow at the respective surfaces such that shielding is less effective.
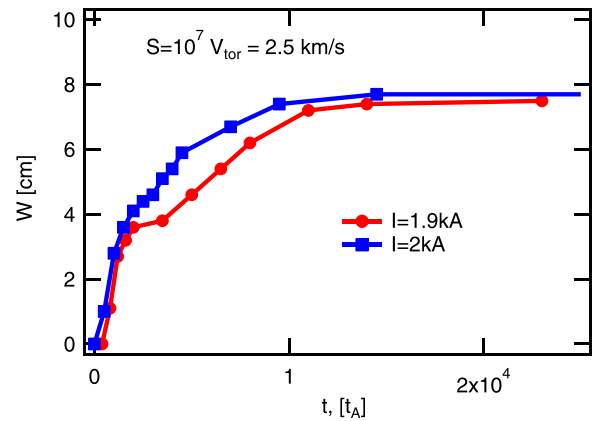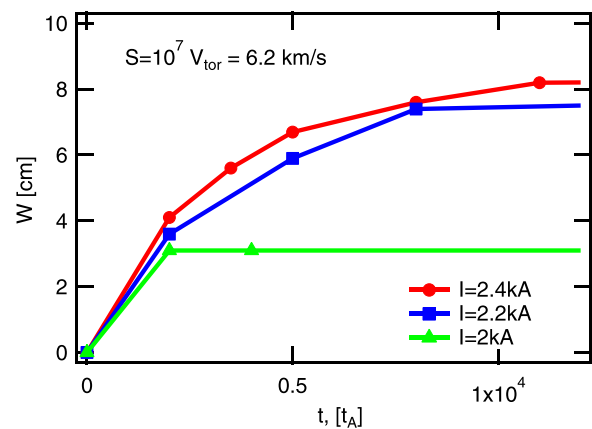

FIG. 15. Island size evolution for different values of the current in RMP coils $V_{tor} = 6.2$ km/s.
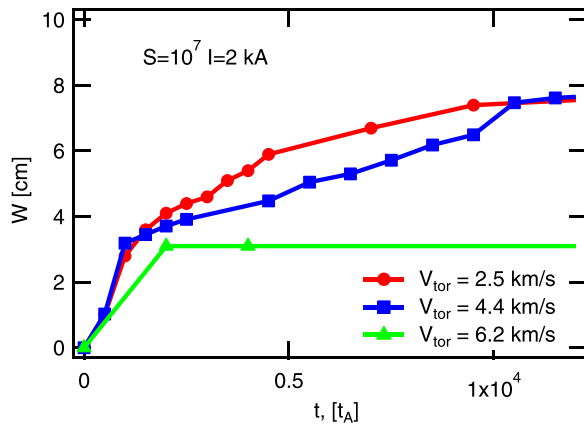
FIG. 16. Island size evolution for different toroidal velocities.

FIG. 17. Hysteresis behavior of the steady state plasma rotation. Initial toroidal rotation velocity $V_{tor} = 6.2$ km/s.

is similar to moving from a lower to an upper curve in Fig. 1. As predicted by the analytical model, if the rotation is strong enough for a given perturbation amplitude, there is no sufficient slowdown of the plasma, and the RMP field thus remains partially screened like for the lower curve in Fig. 16.

It is interesting to point out that, in the case of mode penetration, the final saturated island size is defined solely by the current in RMP coils and is independent of the original plasma velocity. This can be seen in Fig. 16, where the island size follows a universal square-root behavior with respect to the applied coil currents for the penetrated states.

F. Simulation of the hysteresis in mode penetration between current ramp-up and ramp-down

An additional set of simulations was performed to study the analytically predicted hysteresis between current ramp-up and ramp-down. As RMP current and associated $\mathbf{j} \times \mathbf{B}$ torque increase, the steady state value for the perpendicular electron velocity at the rational surface gradually decreases. As seen for the solid curve in Fig. 17, a "jump" is observed to a low rotational state at a coil current of about 2.1 kA. As seen in Fig. 18, this corresponds to a jump to a large island size, thus to mode penetration.

When the coil current is ramped down now again starting from the steady state solution of the simulation with 2.2 kA coil current, the island remains in the penetrated state with low perpendicular electron velocity at the rational surface and large island size significantly longer (dashed line in Figs. 17 and 18). The back transition appears only around a coil current of 1.2 kA. This implies that a decrease in the perturbation amplitude only slightly below the penetration threshold does not cause a significant decrease in the island size. The small drop of the island size is only given by the square-root dependency of the penetrated island size to the perturbation amplitude. In the case of significant pressure gradients, the additional bootstrap current drive can lead to a nonlinearly unstable island such that the island remains present even if the external perturbation is switched off entirely again (NTM). The bootstrap current drive is neglected in the present study due to the low pressure gradients in the considered L-Mode plasma.
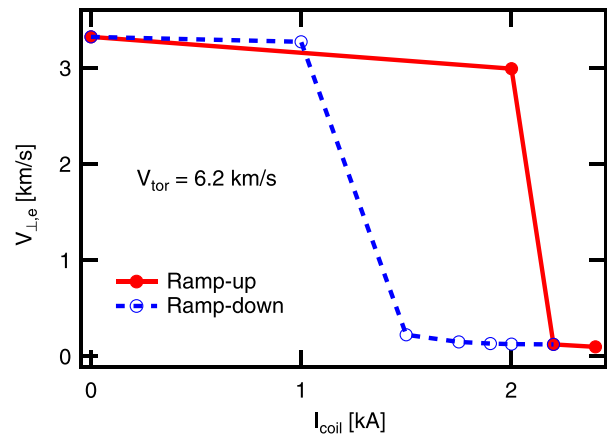
G. Evolution of kink/bending and tearing responses during mode penetration

In this section, the transition from kink/bending[42,45] to tearing responses is briefly investigated for one of our simulations. This topic was discussed before e.g., in Refs. 14, 15, and 43. Figure 19 shows the evolution of the island size over time across the mode penetration time. At the same time, the square-root of $\Psi_{2/1}$ at the rational surface is plotted. Both curves show excellent agreement, verifying that the perturbed poloidal magnetic flux at the rational surface is a very good measure for the island size. This, however, is not necessarily true for magnetic measurements at coil locations where the decay of the signals has to be taken into account properly and the plasma response between the island location and measurement location can additionally alter the signals.

Figure 20 shows how the absolute value of the 2/1 magnetic perturbation grows with time. In Fig. 21, it is depicted how the phase jump of this 2/1 perturbation across the rational surface is changing with time. With phase jump, we refer to the difference of the phase of
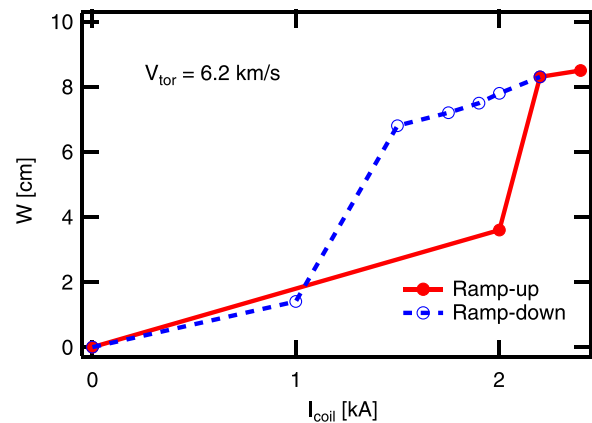

FIG. 18. Hysteresis behavior of the magnetic island size. Initial toroidal rotation velocity $V_{tor} = 6.2$ km/s.
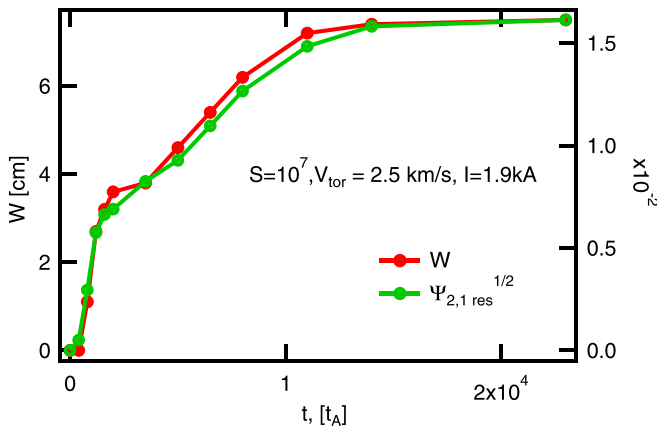
FIG. 19. Time evolution of the island size and the 2/1 component of the magnetic flux.
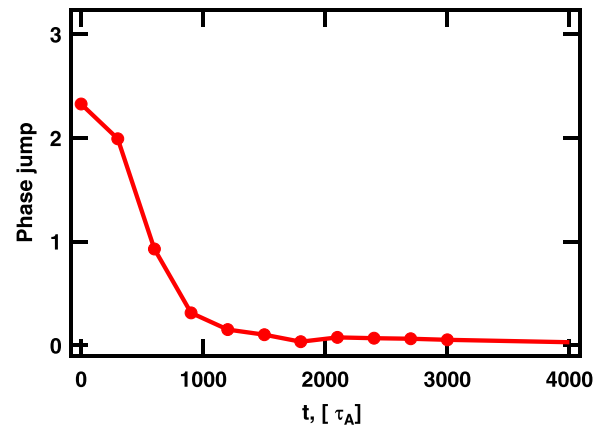

FIG. 21. Time evolution of the phase jump of the 2/1 component of the poloidal flux across the $q = 2$ resonant surface. The difference of the phase of the 2/1 Ψ component between the radial locations $\Psi_N = 0.7$ and $\Psi_N = 0.64$ is plotted. A phase jump close to π refers to a dominant kink/bending parity, while a phase jump close to 0 corresponds to a dominant tearing parity.

approached already after about 1000 Alfvén times, indicates a dominant tearing parity of the magnetic perturbation.

IV. CONCLUSIONS

Tearing mode seeding by magnetic perturbations has been studied in tokamak X-point geometries both experimentally and numerically and was compared with analytical theory. As a source for the magnetic perturbation, resonant magnetic perturbation coils are used although our results are fully transferable to other sources like sawtooth crashes.[44] The simulations were carried out with the nonlinear two-fluid MHD code JOREK. Input parameters close to the experimental ones were chosen; however, simulations were performed at a slightly reduced Lundquist number and increased coil currents. This was done to compensate for missing NTV effects not accounted for in the simulations.

All three phases of mode penetration observed in the experiment were also obtained in the simulations: "weak" response, a fully formed island state, and the transition between these two regimes called penetration. A drop of the core toroidal rotation during the penetration is also observed, similar to experiments; however, the drop in the simulations is weaker due to the absence of NTV in our simulations. The decay of the electron perpendicular velocity is consistent with experimental observations, meaning that the drop of $V_{\perp,e}$ to 0 corresponds to the mode penetration in both cases. The simulation results were compared with the analytical model for MP penetration derived in cylindrical geometry. Scans in the toroidal plasma rotation and perturbation amplitude confirm the analytically predicted thresholds for the fast transition into the low rotation regime. A hysteresis between the RMP current ramp-up and ramp-down was observed like analytically predicted as well. We confirmed a fast formation of the kink/bending response and a delayed tearing response at the rational surface.
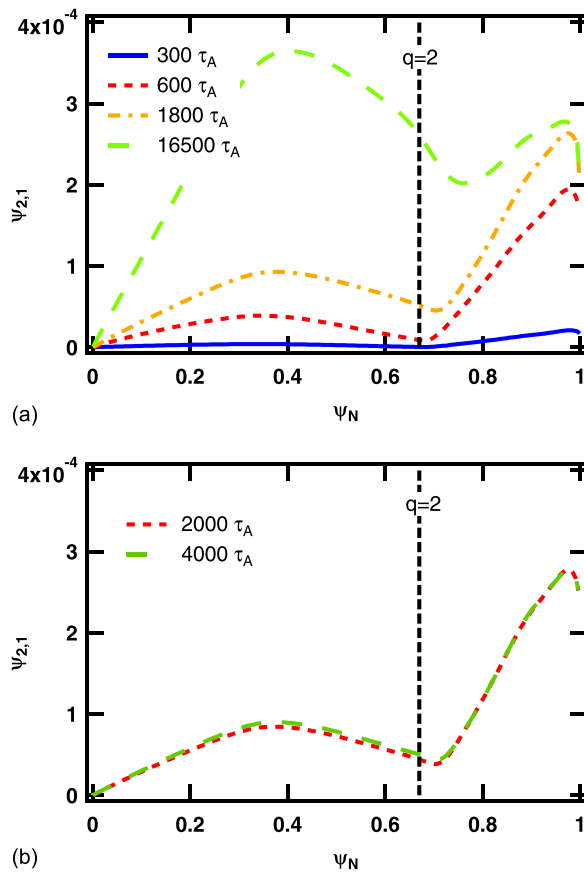
FIG. 20. Radial profiles for the absolute value of the 2/1 component of the poloidal magnetic flux at different time points in the simulation.

the 2/1 poloidal flux between locations outside the rational surface ($\Psi_N = 0.7$) and inside the rational surface ($\Psi_N = 0.64$). A phase jump close to π, as it is seen initially, indicates a dominant kink/bending parity of the magnetic perturbation. A phase jump close to zero, like it is

APPENDIX: NORMALIZATION

We list a few normalization parameters for our simulations for reference. The normalization is described, e.g., in Ref. 46

$$n_{e,0} = 8 \times 10^{19} \, \text{m/s}, \tag{A1}$$

$$m_{ion} = m_D, \tag{A2}$$

$$\rho_0 = 2.7 \times 10^{-7} \, \text{kg/m}^3, \tag{A3}$$

$$\sqrt{\mu_0 \rho_0} = 5.8 \times 10^{-7}, \tag{A4}$$

$$\sqrt{\mu_0/\rho_0} = 2.2, \tag{A5}$$

$$B_0 = 1.9 T. \tag{A6}$$

REFERENCES

[1] D. Biskamp, *Nonlinear Magnetohydrodynamics* (Cambridge University Press, Cambridge, England, 1993).

[2] Z. Chang, E. D. Fredrickson, S. H. Batha, M. G. Bell, R. V. Budny, F. M. Levinton, K. M. McGuire, G. Taylor, and M. C. Zarnstorff, "Neoclassical tearing modes in tokamak fusion test reactor experiments. I. Measurements of magnetic islands and Δ′," Phys. Plasmas **5**(4), 1076–1084 (1998).

[3] A. I. Smolyakov, "Nonlinear evolution of tearing modes in inhomogeneous plasmas," Plasma Phys. Controlled Fusion **35**(6), 657 (1993).

[4] H. Zohm, G. Gantenbein, A. Gude, S. Gnter, F. Leuterer, M. Maraschek, J. Meskat, W. Suttrop, and Q. Yu, "Neoclassical tearing modes and their stabilization by electron cyclotron current drive in ASDEX upgrade," Phys. Plasmas **8**(5), 2009–2016 (2001).

[5] R. Fitzpatrick, "Helical temperature perturbations associated with tearing modes in tokamak plasmas," Phys. Plasmas **2**(3), 825–838 (1995).

[6] J. F. Drake, T. M. Antonsen, A. B. Hassam, and N. T. Gladd, "Stabilization of the tearing mode in high temperature plasma," Phys. Fluids **26**(9), 2509–2528 (1983).

[7] B. D. Scott, J. F. Drake, and A. B. Hassam, "Nonlinear stability of drift-tearing modes," Phys. Rev. Lett. **54**, 1027–1030 (1985).

[8] B. D. Scott and A. B. Hassam, "Analytical theory of nonlinear drift tearing mode stability," Phys. Fluids **30**(1), 90–101 (1987).

[9] F. L. Waelbroeck, "Current sheets and nonlinear growth of the m = 1 kink-tearing mode," Phys. Fluids B: Plasma Phys. **1**(12), 2372–2380 (1989).

[10] D. Meshcheriakov, P. Maget, H. Ltjens, P. Beyer, and X. Garbet, "Linear stability of the tearing mode with two-fluid and curvature effects in tokamaks," Phys. Plasmas **19**(9), 092509 (2012).

[11] A. Gude, S. Günter, S. Sesnic, and ASDEX Upgrade Team, "Seed island of neoclassical tearing modes at ASDEX upgrade," Nucl. Fusion **39**(1), 127 (1999).

[12] O. Sauter, R. J. Buttery, R. Felton, T. C. Hender, and D. F. Howell, and Contributors to the EFDA-JET Workprogramme, "Marginal β-limit for neoclassical tearing modes in jet h-mode discharges," Plasma Phys. Controlled Fusion **44**(9), 1999 (2002).

[13] R. J. La Haye, "Neoclassical tearing modes and their control," Phys. Plasmas **13**(5), 055501 (2006).

[14] V. Igochine, A. Gude, S. Gnter, K. Lackner, Q. Yu, L. Barrera Orte, A. Bogomolov, I. Classen, R. M. McDermott, N. C. Luhmann, Jr., and ASDEX Upgrade Team, "Conversion of the dominantly ideal perturbations into a tearing mode after a sawtooth crash," Phys. Plasmas **21**, 110702 (2014).

[15] V. Igochine, I. Classen, M. Dunne, A. Gude, S. Gnter, K. Lackner, R. M. McDermott, M. Sertoli, D. Vezinet, M. Willensdorfer, Q. Yu, H. Zohm, and ASDEX Upgrade Team, "Tearing mode formation induced by internal crash events at different β_n," Nucl. Fusion **57**(3), 036015 (2017).

[16] G. Ara, B. Basu, B. Coppi, G. Laval, M. N. Rosenbluth, and B. V. Waddell, "Magnetic reconnection and m = 1 oscillations in current carrying plasmas," Ann. Phys. **112**, 443–476 (1978).

[17] F. L. Waelbroeck, J. W. Connor, and H. R. Wilson, "Finite larmor-radius theory of magnetic island evolution," Phys. Rev. Lett. **87**(21), 215003 (2001).

[18] A. H. Glasser, J. M. Greene, and J. L. Johnson, "Resistive instabilities in tokamak," Phys. Fluids **19**, 567–574 (1976).

[19] R. Fitzpatrick, "Interaction of tearing modes with external structures in cylindrical geometry," Nucl. Fusion **33**(7), 1049 (1993).

[20] E. Nardon, P. Tamain, M. Bcoulet, G. Huysmans, and F. L. Waelbroeck, "Quasi-linear MHD modelling of h-mode plasma response to resonant magnetic perturbations," Nucl. Fusion **50**, 034002 (2010).

[21] F. Orain, M. Hoelzl, E. Viezzer, M. Dunne, M. Bécoulet, P. Cahyna, G. T. A. Huijsmans, J. Morales, M. Willensdorfer, W. Suttrop, A. Kirk, S. Pamela, S. Günter, K. Lackner, E. Strumberger, A. Lessig, the ASDEX Upgrade Team1 and the EUROfusion MST1 Team, "Non-linear modeling of the plasma response to RMPs in ASDEX Upgrade," Nucl. Fusion **57**, 022013 (2017).

[22] G. T. A. Huysmans and O. Czarny, "MHD stability in x-point geometry: Simulation of ELMs," Nucl. Fusion **47**(7), 659 (2007).

[23] O. Czarny and G. Huysmans, "Bezier surfaces and finite elements for MHD simulations," J. Comput. Phys. **227**(16), 7423–7445 (2008).

[24] F. Orain, M. Bécoulet, G. Dif-Pradalier, G. Huijsmans, S. Pamela, E. Nardon, C. Passeron, G. Latu, V. Grandgirard, A. Fil, A. Ratnani, I. Chapman, A. Kirk, A. Thornton, M. Hoelzl, and P. Cahyna, "Non-linear magnetohydrodynamic modeling of plasma response to resonant magnetic perturbations," Phys. Plasmas **20**(10), 102510 (2013).

[25] S. Fietz, R. Coelho, I. Classen, M. Maraschek, W. Suttrop, H. Zohm, the EUROfusion MST1 Team, and the ASDEX Upgrade Team, "Study of suppressed tearing modes seeded with non-axisymmetric magnetic perturbation fields at the ASDEX upgrade tokamak," in *Proceedings of the 42nd EPS Conference on Plasma Physics* (2015), p. P1.123.

[26] A. Kallenbach, ASDEX Upgrade Team, and EUROfusion MST1 Team, "Overview of ASDEX Upgrade results," Nucl. Fusion **57**(10), 102015 (2017).

[27] S. Fietz, A. Bergmann, I. Classen, M. Maraschek, M. Garcia-Munoz, W. Suttrop, H. Zohm, and the ASDEX Upgrade Team, "Influence of externally applied magnetic perturbations on neoclassical tearing modes at ASDEX Upgrade," Nucl. Fusion **55**(1), 013018 (2015).

[28] E. Viezzer, T. Pütterich, R. Dux, and R. M. McDermott, "High-resolution charge exchange measurements at ASDEX Upgrade," Rev. Sci. Instrum. **83**(10), 103501 (2012).

[29] R. M. McDermott, C. Angioni, G. D. Conway, R. Dux, E. Fable, R. Fischer, T. Putterich, F. Ryter, E. Viezzer, and the ASDEX Upgrade Team, "Core intrinsic rotation behaviour in ASDEX Upgrade ohmic l-mode plasmas," Nucl. Fusion **54**, 043009 (2014).

[30] E. Viezzer, T. Ptterich, C. Angioni, A. Bergmann, R. Dux, E. Fable, R. M. McDermott, U. Stroth, and E. Wolfrum, "Evidence for the neoclassical nature of the radial electric field in the edge transport barrier of ASDEX Upgrade," Nucl. Fusion **54**(1), 012003 (2014).

[31] F. L. Waelbroeck, "Shielding of resonant magnetic perturbations in the long mean-free path regime," Phys. Plasmas **10**(10), 4040–4047 (2003).

[32] E. Nardon, M. Bécoulet, G. Huysmans, and O. Czarny, "Magnetohydrodynamics modelling of h-mode plasma response to external resonant magnetic perturbations," Phys. Plasmas **14**(9), 092501 (2007).

[33] M. F. Heyn, I. B. Ivanov, S. V. Kasilov, W. Kernbichler, I. Joseph, R. A. Moyer, and A. M. Runov, "Kinetic estimate of the shielding of resonant magnetic field perturbations by the plasma in DIII-d," Nucl. Fusion **48**(2), 024005 (2008).

[34] M. Bécoulet, F. Orain, G. T. A. Huijsmans, S. Pamela, P. Cahyna, M. Hoelzl, X. Garbet, E. Franck, E. Sonnendrücker, G. Dif-Pradalier, C. Passeron, G. Latu, J. Morales, E. Nardon, A. Fil, B. Nkonga, A. Ratnani, and V. Grandgirard, "Mechanism of edge localized mode mitigation by resonant magnetic perturbations," Phys. Rev. Lett. **113**, 115001 (2014).

[35]H. R. Strauss, "Reduced MHD in nearly potential magnetic fields," J. Plasma Phys. **57**(1), 83–87 (1997).

[36]E. Franck, M. Hoelzl, A. Lessig, and E. Sonnendrücker, "Energy conservation and numerical stability for the reduced MHD models of the non-linear JOREK code," ESAIM **49**(5), 1331–1365 (2015).

[37]R. D. Hazeltine, M. Kotschenreuther, and P. J. Morrison, "A four-field model for tokamak plasma dynamics," Phys. Fluids **28**(8), 2466–2477 (1985).

[38]T. A. Gianakon, S. E. Kruger, and C. C. Hegna, "Heuristic closure for numerical simulations of neoclassical tearing modes," Phys. Plasmas **9**(2), 536–547 (2002).

[39]L. Spitzer and R. Härm, "Transport phenomena in a completely ionized gas," Phys. Rev. **89**, 977–981 (1953).

[40]R. C. Malone, R. L. McCrory, and R. L. Morse, "Indications of strongly flux-limited electron thermal conduction in laser-target experiments," Phys. Rev. Lett. **34**, 721–724 (1975).

[41]M. Hölzl, S. Günter, I. G. J. Classen, Q. Yu, the TEXTOR Team, and E. Delabie, "Determination of the heat diffusion anisotropy by comparing measured and simulated electron temperature profiles across magnetic islands," Nucl. Fusion **49**(11), 115009 (2009).

[42]Note 1. The term bending is preferred e.g., in Ref. 45 over kinking; we use both terms synonymously since both of them are common in literature.

[43]Q. Yu, S. Günter, K. Lackner, and M. Maraschek, "Seed island formation by forced magnetic reconnection," Nucl. Fusion **52**, 063020 (2012).

[44]J. Loizu and P. Helander, "Unified nonlinear theory of spontaneous and forced helical resonant mhd states," Phys. Plasmas **24**, 040701 (2017).

[45]N. M. Ferraro, "Calculations of two-fluid linear response to non-axisymmetric fields in tokamaks," Phys. Plasmas **19**, 056105 (2012).

[46]M. Hölzl, S. Günter, R. P. Wenninger, W.-C. Mueller, G. T. A. Huysmans, K. Lackner, and I. Krebs, and ASDEX Upgrade Team, "Reduced-MHD simulations of toroidally and poloidally localized ELMs," Phys. Plasmas **19**, 082505 (2012).